JOURNAL OF MATERIALS SCIENCE 2 (1967) 521–528

Measurement of Particle Size, Volume Fraction, and Foil Thickness from Electron Microscopic Observations

C. M. SELLARS
Department of Metallurgy, The University, Sheffield, UK

A. F. SMITH
Central Electricity Generating Board, Berkeley Nuclear Laboratories, Berkeley, Glos, UK

Received 15 May 1967

The analysis of images produced by thin foils containing dispersed spherical particles is developed for the case when particles which intersect the foil surface remain unattacked during thinning. Identification of these particles is shown to allow quantitative assessment of the second phase and the foil thickness. The model is tested and experimental techniques for labelling surface particles are discussed with reference to data on aged Mg/0.67 wt % Mn.

1. Introduction

The interpretation of images produced by transmission electron microscopy of thin foils containing dispersed particles has been considered by several authors. Cahn and Nutting [1] and Hilliard [2] described corrections which must be made for the overlap of images when the mean particle diameter is small compared with the foil thickness. These authors and, more recently, Crompton *et al* [3] have also discussed in detail the corrections which must be made for particles which intersect the foil surface but have their centres lying outside the foil. In all these analyses, it was assumed that particles intersecting the foil surface were sectioned in the plane of the surface. Although this assumption may be true in some experimental situations, it is not likely to be generally valid because of non-uniform electrolytic thinning of the two phases. Usually particles will be left either at virtually their original diameter or preferentially dissolved.

We assume that the usual situation is represented by fig. 1, where the foil is an approximately flat, parallel slice of the matrix, in which all particles which intersect the surface are retained at their original diameter within the volume. Analysis of the images from such a foil is considered, and the model is then tested by applying it to a dispersion of approximately spherical manganese particles in a magnesium matrix.

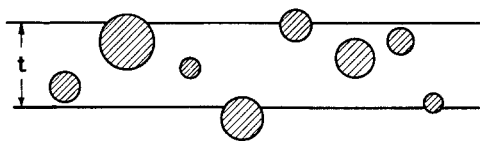

Figure 1 Schematic representation of a section through a thin foil containing second-phase particles.

2. Analysis

2.1. Particle Diameters

The particles are assumed to be spherical with a mean particle size which is a fairly large fraction of the foil thickness. Thus, for small volume fractions, overlap of images is negligible and near-overlaps can be easily detected. Under these conditions, although there is no error due to dissolution of particles, the true distribution of particles diameters in the volume is not given by the total distribution of image sizes. As a significant fraction of images originates from particles having their centres outside the foil, the total distribution is influenced by the fact that the distribution of particle sizes intersecting

a plane is not the same as the distribution of sizes within the volume [4].

Consider a distribution of particle diameters within the volume, such that there are n_i particles of diameter $d_i \pm \frac{1}{2}\delta d$ per unit volume; where the group size δd is small compared with the standard deviation of diameters so that grouping errors are not introduced. The true mean particle diameter $\bar{d}$ is then simply

$$\bar{d} = \Sigma n_i d_i / \Sigma n_i \quad (1)$$

If a unit plane is drawn at random through this volume, the number, m_i, of particles of diameter d_i which is intersected is [5, 6]

$$m_i = n_i d_i \quad (2)$$

and half these particles have their centres above the plane and half below it.

Thus, from a thin foil of thickness t, the total number of images per unit area from particles of diameter d_i will be

$$n_i^A = tn_i + m_i = n_i(t + d_i) \quad (3)$$

To obtain the true volume distribution of particle sizes, it is therefore necessary to know the average foil thickness over the area observed. Although there are several experimental techniques by which an independent measure of foil thickness may be obtained [7-9], the necessary structural features are frequently not present in the examined areas of foils containing dispersed particles.

An alternative approach is to label those particles which intersect one or both of the foil surfaces.

(*a*) Particles which intersect one foil surface only are labelled. In this case, as an equal number of particles of diameter d_i should intersect each surface, the number of labelled particles will be equal to the number which have their centres outside the foil. Therefore, if only the unlabelled images are measured, the number of images per unit area from particles of diameter d_i will be

$$n_i^B = tn_i \quad (4)$$

Thus the true volume distribution of particle diameters is given directly by the distribution of image diameters.

(*b*) Particles which intersect both foil surfaces are labelled, but those intersecting one surface cannot be distinguished from those intersecting the other. In this case, the labelled and unlabelled images must be measured separately. The number of images per unit area from unlabelled particles (i.e. particles entirely within the foil) of diameter d_i will be

$$n_i^C = tn_i - m_i \quad (5)$$

and the number of images per unit area from labelled particles of diameter d_i will be $m_i^C = 2m_i$. Therefore the true distribution of particle sizes in the volume may be obtained from the distributions of labelled and unlabelled images as

$$tn_i = n_i^C + \tfrac{1}{2}m_i^C \quad (6)$$

2.2. Volume Fraction and Foil Thickness

Summing equation 3 over all particle diameters gives the total number of images per unit area:

$$N^A = \Sigma n_i^A = N_v(t + \bar{d}) \quad (7)$$

where N_v ($=\Sigma n_i$) is the number of particles per unit volume. This is the expression given by Cahn and Nutting [1] and by Hilliard [2] when the overlap correction is negligible. Similarly, summing equation 4 gives the number of images per unit area from particles with centres inside the foil:

$$N^B = \Sigma n_i^B = N_v t \quad (8)$$

and summing equation 5 gives the number of images per unit area from particles entirely within the foil:

$$N^C = \Sigma n_i^C = N_v(t - \bar{d}) \quad (9)$$

Thus, when $\bar{d}$ has been determined, if the procedures outlined in (*a*) or (*b*) above are followed, so that N^A and N^B, or N^A and N^C are known, both N_v and the average foil thickness t may be obtained directly by simultaneous solution of equations 7 and 8, or 7 and 9.

When t and hence n_i are known, the volume fraction of second phase is simply obtained as

$$f = \pi \Sigma n_i d_i^3 / 6 \quad (10)$$

3. Experimental

A series of Mg/0.67 wt % Mn alloys, which had been hot-worked in the two-phase region and then aged for various times in the temperature range 350 to 450° C, were prepared as thin foils by chemical thinning in dilute nitric acid followed by careful cleaning to remove particles lying loosely on the surfaces. Foils were examined in a Siemens Elmiscop I electron microscope.

Images observed from the as-prepared foils were typically as shown in fig. 2a. The second-phase particles of virtually pure manganese are

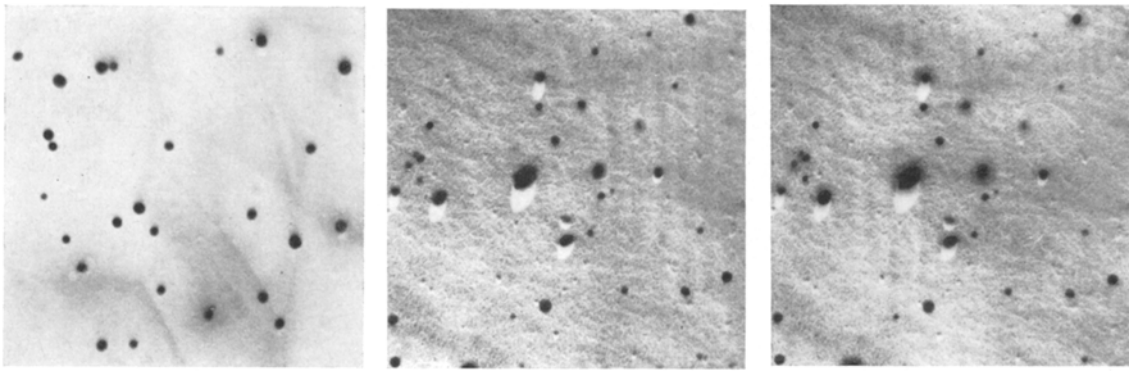

(a) (b) (c)

Figure 2 Thin foils of Mg/0.67 wt % Mn alloy aged for 340 h at 400° C (×26 500): (a) as-thinned; (b) shadowed with gold/palladium at ~25°; (c) same area as (b) after contamination in the microscope.

seen to be approximately spherical and fairly uniformly distributed. Near-overlaps are infrequent and are easily detected, indicating that overlap errors will be small. At this stage, it is not possible to distinguish the particles entirely within the foil from those which intersect the surface.

In order to label particles intersecting one surface, the foil was lightly shadowed with gold/palladium at an angle of about 25° before examination in the microscope. The image obtained from such a foil is shown in fig. 2b. Certain particles are now distinguishable by their shadows. This shows clearly that the particles are not sectioned at the foil surface, and the variation in length of shadow for a given particle size indicates that the particle centres are distributed both above and below the foil surface. The lack of surface features over the remainder of the foil indicates that, on the scale of the particles, the surface is smooth and relatively flat, and that no particles have been displaced from the surface. Consideration of the geometry of shadowing (Appendix) shows that, under the present experimental conditions, about 85% of the particles intersecting the shadowed surface should cast visible shadows and so be clearly labelled.

If the foil is allowed to become contaminated in the microscope, the image obtained is as shown in fig. 2c. All the particles with shadows now have "halos" as well, owing to the build-up of contamination around them. A number of particles without shadows have also developed halos, indicating that they intersect the bottom surface of the foil.

Halos produced in this way have previously been used to distinguish qualitatively particles which intersect the surface of unshadowed foils [10]. To determine whether halos could be used for quantitative labelling, the nature of the contamination build-up has been examined by shadowing foils which had previously been exposed in the microscope. Fig. 3 shows the appearance after such treatment of a particle which intersects the foil surface. This indicates that the contamination builds up in the form of a segment of a sphere around the particle. The thickness of contamination around particles of different size was observed to be about the same, but a considerable variation in length of shadow was found for particles of similar size. This suggests that the height of the spherical segment of contamination is determined by the position of the centre of the particle relative to the foil surface. Confirmation of this is obtained from

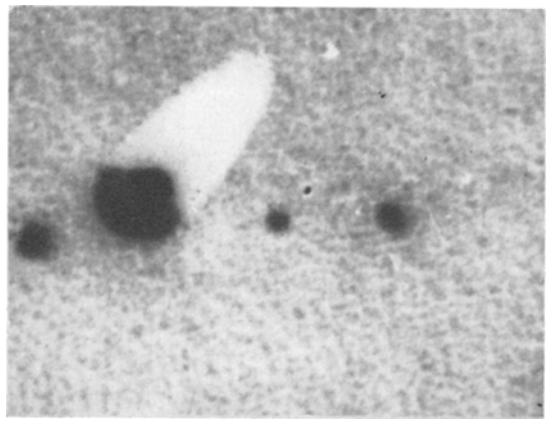

Figure 3 Thin foil of Mg/0.67 wt % Mn alloy aged for 24 h at 446° C; foil contaminated in the microscope, then shadowed with gold/palladium at ~25° (×100 000).

foils shadowed prior to exposure in the microscope (cf. fig. 2c), as halos which form around particles with long shadows have a higher density than those around particles with short shadows, showing that the depth of contamination penetrated by the beam is greater in the former case. Thus the geometry of contamination appears to be simply related to that of the particle, and consideration of the conditions for visibility of a halo (Appendix) shows that about 85% of the particles which intersect the surface should be labelled after sufficient exposure in the microscope.

Results from several shadowed and contaminated foils taken from material aged at different temperatures are listed in table I. These show that, although the number of particles observed in a given area of foil varied widely, the number of particles with shadows is always approximately equal to the number with halos only. Thus the reliability of labelling by shadows and by halos is similar, and the number of particles intersecting one surface is always approximately the same as that intersecting the other. The assumption made in the analysis – that the particles are randomly distributed in the thickness of the foil – therefore appears to be realistic even when the total number of particles observed in a given area is small.

The diameters of particles within the foil and of those intersecting the surfaces were measured separately, and the mean diameter was determined for particles which have their centres within the foil, i.e.

$$\bar{d} = \frac{\Sigma(n_i^C + \frac{1}{2} m_i^C)\, d_i}{\Sigma(n_i^C + \frac{1}{2} m_i^C)}$$

No correction was made for the fact that some particles which intersect the surfaces are not labelled, as the size of these particles is not known. However, this leads to a negligible error in the present case, as the confidence limits of the means are much greater than the systematic error introduced if the mean is calculated from all observed particles. The mean diameters are found to vary significantly from area to area, particularly when the area observed is small. Thus, although the overall mean is determined to about $\pm 4\%$ if all the particles are assumed to originate from the same population, the confidence limits are much wider if the overall mean is calculated from the individual area means (figures in brackets in the table).

Foil thicknesses were determined from equations 7 and 9 after correction of the number of labelled particles, to allow for the fact that labelling is only about 85% efficient. The foils varied from about 650 to 2200 Å in thickness, with an overall average of about 1250 Å. Fig. 4a shows that there is not a significant correlation between foil thickness and mean particle diameter, even though the latter is involved in the determination of thickness.

The number of particles per unit volume, calculated from the corrected particle distributions, varies widely. Fig. 4c shows that there is a significant correlation between the number of particles per unit volume in a given volume of foil and the mean particle diameter in that volume. If it is assumed that, during coarsening, the distribution of $d/\bar{d}$ is constant [11], it follows that, for constant volume fraction, $N_v\bar{d}^3$ is constant. Thus fig. 4c shows that, although there are significant variations in particle size from region to region, the number of particles varies in such a way that the mean volume fraction is constant, indicating that the alloys are not segregated. This is confirmed by the measured volume fractions which show no significant correlation with the local mean particle diameter (fig. 4b).

As the volume fraction determined depends on the value of foil thickness, this may be used as a check on the validity of the values obtained. In fig. 5, the solubility limits calculated from the total manganese content, and the volume fraction of second phase are compared with published data [12-14]. The results are in reasonable agreement and show no systematic error. Thus there is little systematic error in the foil-thickness measurements. This also shows that there is an insignificant number of loose particles resting on the foil surfaces, for these would lead to low values of foil thickness and high values of the volume of particles, and so to a systematic increase in the measured volume fractions. The random error in the foil-thickness measurements cannot easily be estimated, as the parameters used in the calculation are not independent variables. However, a reasonable estimate would be that the standard error is about twice that of the mean particle diameter (i.e. about $\pm 10\%$).

4. Conclusions

(*a*) A model of a thin foil in which second-phase particles intersecting the surface are complete appears to be more realistic than one

TABLE I Quantitative assessment of second-phase particles in aged Mg/Mn alloys.

Area	Number of particles			$\bar{d} \pm 95\%$ CL*	t	N_v	f
($cm^2 \times 10^{-8}$)	Clean	Shadows	Halos only	(Å)	(Å)	($10^{12}/cm^3$)	($\times 10^3$)
0.67 wt % Mn aged 285 h at 350° C							
5.1	38	8	9	334 ± 34	1510	58	1.14
4.9	40	10	10	313 ± 30	1260	78	1.78
5.3	74	19	17	245 ± 20	1040	158	1.95
5.1	29	9	7	368 ± 38	1380	50	1.52
5.3	32	8	8	294 ± 45	1200	60	1.42
5.0	43	7	9	321 ± 33	1670	59	1.40
Mean	42.7	9.8	10.0	301 ± 13	1340	77	1.53
95% CL				(312 ± 79)		±43	±0.30
0.68 wt % Mn aged 2850 h at 350° C							
13.4	40	16	20	396 ± 25	1040	39	1.76
12.9	42	20	20	357 ± 26	880	51	1.62
12.4	40	15	18	370 ± 26	1020	42	1.47
13.1	40	11	17	426 ± 38	1330	30	1.65
13.4	38	13	13	425 ± 36	1330	33	1.51
13.1	53	24	23	370 ± 28	980	56	1.70
Mean	42.2	16.5	18.5	388 ± 12	1100	42	1.62
95% CL				(391 ± 31)		±11	±0.12
0.67 wt % Mn aged 340 h at 400° C							
12.9	35	13	11	397 ± 33	1270	27	1.14
12.9	46	14	15	387 ± 33	1320	34	1.24
13.0	53	13	13	342 ± 31	1400	35	1.09
13.1	32	13	12	407 ± 34	1210	27	1.24
13.0	67	12	12	353 ± 24	2190	27	0.84
13.1	11	8	12	465 ± 40	740	20	1.23
Mean	40.7	12.2	12.5	378 ± 13	1350	28	1.13
95% CL				(392 ± 47)		± 6	±0.16
0.67 wt % Mn aged 24 h at 446° C							
12.7	18	8	8	344 ± 24	890	21	0.52
12.7	19	11	10	335 ± 27	740	29	0.71
13.1	30	14	12	375 ± 28	980	32	1.26
13.0	35	10	8	372 ± 34	1520	21	0.78
11.4	36	6	7	373 ± 30	2060	18	0.58
13.0	13	9	8	329 ± 39	660	23	0.57
Mean	25.2	8.8	9.7	360 ± 13	1140	24	0.74
95% CL				(354 ± 19)		± 6	±0.29

*95% confidence limits of mean

in which the particles are sectioned at the foil surface.

(*b*) Particles which intersect one surface of a foil can be labelled by shadowing; or particles which intersect either surface can be labelled by allowing contamination in the microscope. Either technique allows a complete quantitative assessment to be made of the second-phase particles in the volume.

(*c*) The mean foil thickness over the area

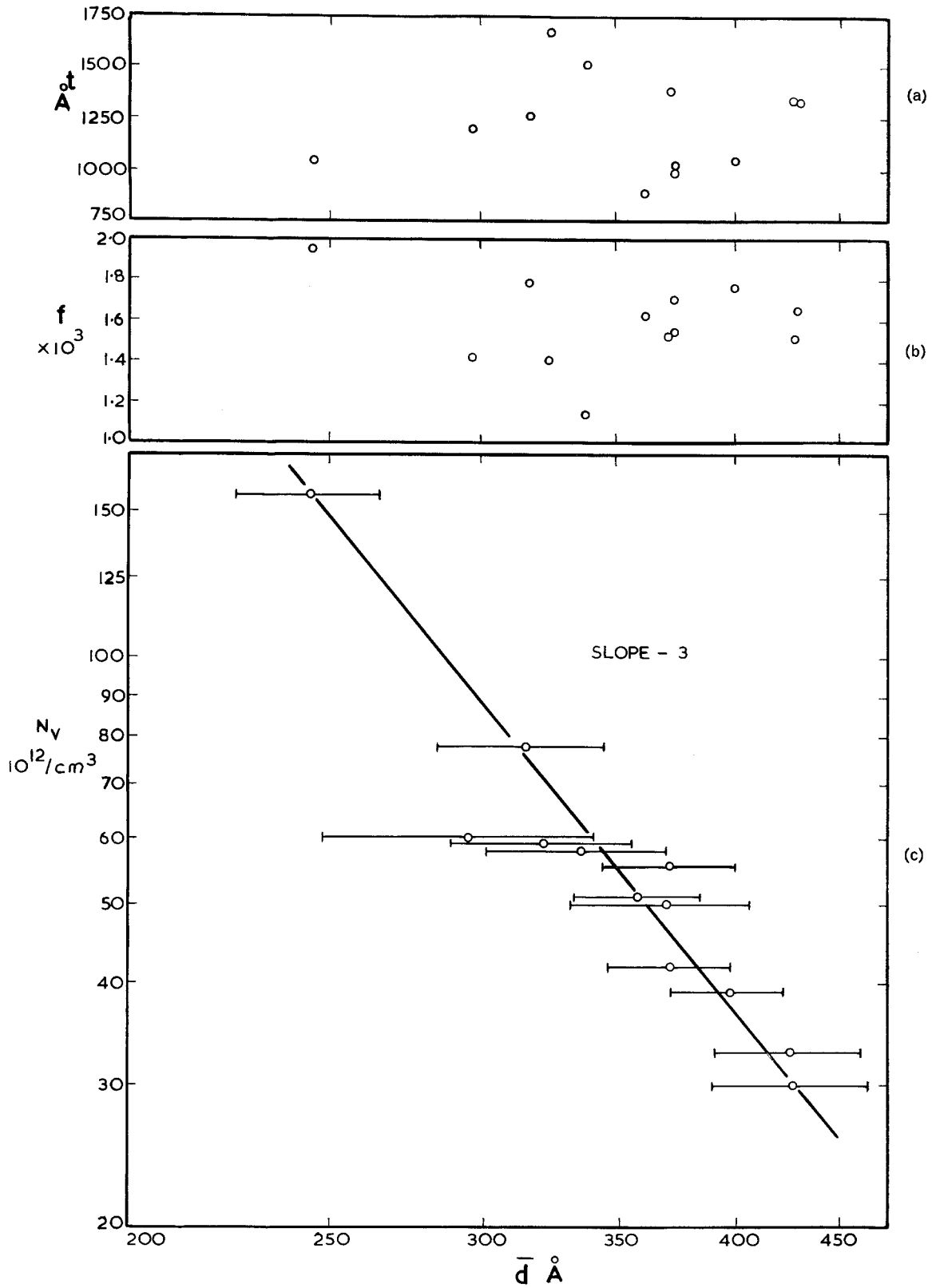

Figure 4 Relationship between: (a) foil thickness; (b) volume fraction; (c) number of particles per unit volume and mean particle diameter – Mg/0.67 to 0.68 wt % Mn aged at 350° C.

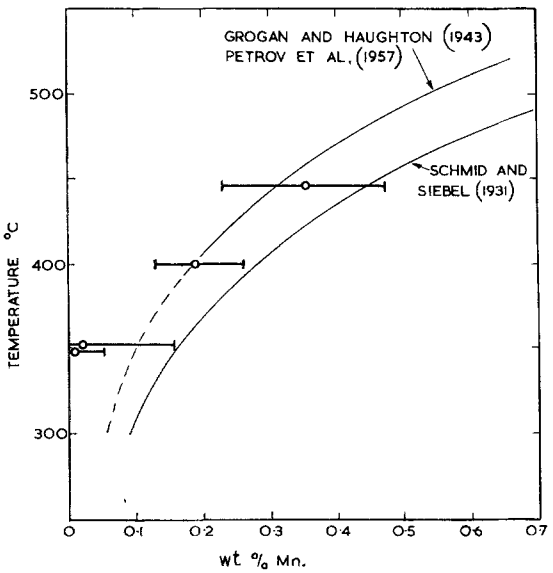

Figure 5 Solubility limit of manganese in magnesium.

observed can be determined from the analysis to an accuracy comparable to that of other techniques.

Appendix

Visibility of shadows For a particle which intersects the surface to cast a visible shadow, the shadow must extend beyond the diameter of the particle. The limiting condition, shown in fig. 6a, gives that, for visibility,

$$h/r > 1 + \tan\theta - \sec\theta$$

Thus, for shadowing angles of 15, 20, and 25°, the percentages of randomly distributed particles which are intersected by the surface, but do not cast visible shadows, are 12, 15, and 18%, respectively.

The true angle of shadowing with respect to the foil surface may differ from the nominal angle because of bending of the foil or tilting with respect to the grid. If the longest observed shadow is assumed to originate from a particle which is virtually in contact with the surface, the true angle of shadowing can be estimated.

If, as indicated in fig. 6a, the shadow is of length ar, then

$$ar \tan\theta = 2r - h$$

so

$$\cos\theta = [(1 + a)^2 - 1]/[(1 + a)^2 + 1]$$

In the present case, the angle was found to vary between about 15 and 25°; so ~15% of

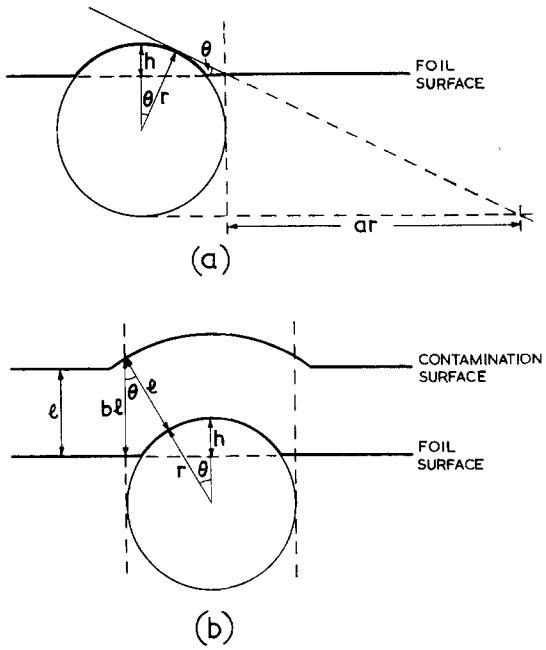

Figure 6 Geometry of (a) shadowing and (b) contamination, showing the limiting conditions for effective labelling.

particles which intersect the shadowed surface are not expected to develop visible shadows.

Visibility of halos For the contamination around a particle which intersects the surface to be visible, the thickness of contamination through which the electrons pass must be significantly greater than that over the surface of the foil as a whole. The geometry of contamination is shown in fig. 6b, where the condition for visibility is that the electrons must pass through a thickness bl of contamination at the maximum section of the particle, i.e.

$$(r + l)\sin\theta > r$$

when

$$(r + l)\cos\theta = r - h + bl$$

Thus for visibility,

$$(r + l)^2 > r^2 + (r + bl - h)^2$$

If $l = r$ and $b = 1.05$ then $h/r = 0.30$
,, $l = 2r$,, $b = 1.05$,, $h/r = 0.26$
,, $l = r$,, $b = 1.10$,, $h/r = 0.35$
,, $l = 2r$,, $b = 1.10$,, $h/r = 0.35$

In the present work, l is between about r and $2r$ for most particles. Therefore, with randomly distributed particles, ~15% of those which

intersect the surface are not expected to develop visible halos.

Acknowledgement

This paper is published by permission of the Central Electricity Generating Board.

References

1. J. W. CAHN and J. NUTTING, *Trans. AIME* **215** (1959) 526.
2. J. E. HILLIARD, *ibid* **224** (1962) 906.
3. J. M. G. CROMPTON, R. M. WAGHORNE, and G. B. BROOK, *Brit. J. Appl. Phys.* **17** (1966) 1301.
4. M. F. ASHBY and R. EBELING, *Trans. AIME* **236** (1966) 1396.
5. E. SCHEIL, *Z. Metalk.* **27** (1935) 119.
6. R. L. FULLMAN, *Trans. AIME* **197** (1953) 447.
7. P. B. HIRSCH, A. HOWIE, R. B. NICHOLSON, D. W. PASHLEY, and M. J. WHELAN, "Electron Microscopy of Thin Crystals" (Butterworths, London, 1965), p. 415.
8. C. L. FORMBY, *Phil. Mag.* **13** (1966) 621.
9. Y. ISHIDA, *ibid* **14** (1966) 411.
10. J. E. HARRIS, P. G. PARTRIDGE, W. J. EELES, and G. K. RICKARDS, *J. Nucl. Matls.* **9** (1963) 339.
11. C. WAGNER, *Z. Elektrochem.* **65** (1961) 581.
12. E. SCHMID and G. SIEBEL, *Metallwirtschaft* **10** (1931) 923.
13. J. D. GROGAN and J. L. HAUGHTON, *J. Inst. Metals* **69** (1943) 241.
14. D. A. PETROV, M. S. MIRGALOVSKAYA, I. A. STRELNITCOVA, and E. M. COMAVA, *Trudy Inst. Metall. A A Baukova, Akad. Nauk. SSSR* **1** (1957) 142.